

Dawson-Type Vanadium-Substituted Tungstophosphate-Modified ITO Electrode: Preparation, Characterization and Electrochemical Determination of Dopamine

Xinming Wang¹, Yuanqing Zhao¹, Di Zhang^{1,2}, Shuang Rong³, Huiyuan Ma^{1,*}

¹ Key Laboratory of Green Chemical Engineering and Technology of College of Heilongjiang Province, College of Chemical and Environmental Engineering, Harbin University of Science and Technology, Harbin 150040, China

² School of Materials Science and Engineering, Harbin Institute of Technology, Harbin 150001, China

³ Heilongjiang electric power research institute, Harbin 150032, China

*E-mail: mahy017@163.com

Received: 19 November 2018 / Accepted: 17 January 2019 / Published: 10 March 2019

In this work, we describe a robust composite film-modified indium tin oxide (ITO) electrode with improved detection capabilities for an example neurotransmitter, dopamine (DA). The composite film was developed by the combination of a Dawson-type vanadium tungstophosphate, α_2 -K₇P₂W₁₇VO₆₂·18H₂O (P₂W₁₇V), and cationic chitosan (CS) via a layer-by-layer (LbL) self-assembly technique. The composite film-modified electrode presents excellent electrochemical catalytic activity towards dopamine (DA) with a linear response over the range of 1.25×10^{-8} M to 3.04×10^{-4} M. The proposed system responds selectively to dopamine with a low detection limit of 0.18 μ M (S/N = 3), a high sensitivity of 0.23 μ A μ M⁻¹ and a quick response time. As a result, the prepared composite film materials with these superior properties show promising applicability in electrochemical sensors.

Keywords: composite film; polyoxometalate; electrochemistry; dopamine

1. INTRODUCTION

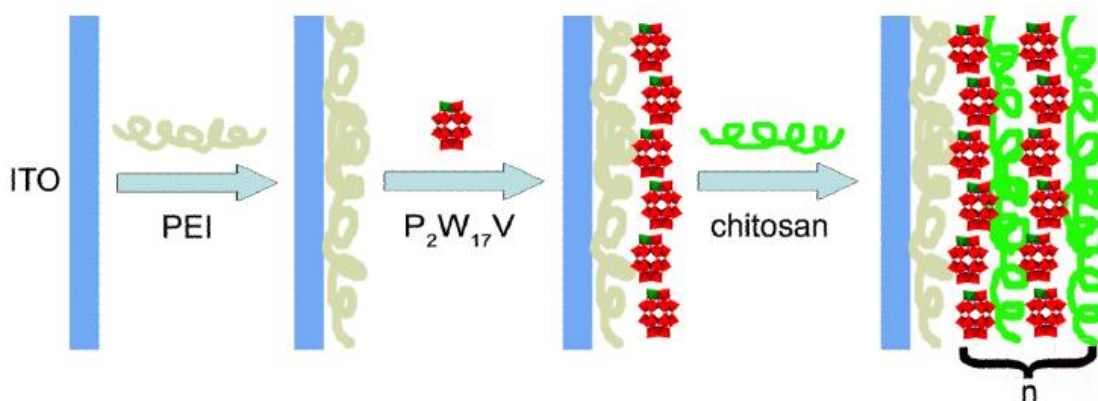
Dopamine (DA) has been considered an important neurotransmitter in mammalian central nervous systems since its discovery in the 1950s [1]. Several diseases and neurological disorders have been attributed to a lack of DA, such as Alzheimer's disease, Parkinson's disease, schizophrenia and human immunodeficiency virus pathogenesis [2, 3]. Therefore, it is important to determine the DA level sensitively and selectively improve human health. Over the past few decades, high-performance

liquid chromatography (HPLC) [4], capillary electrophoresis [5], fluorescence [6], and electrochemical methods [7–8], for instance, have been used to detect DA levels.

Among the various techniques used for the detection of DA, electrochemical methods are of interest due to their quick reaction times and high sensitivity; additionally, the easy electrooxidation of DA increases the applicability of these methods. However, in the extracellular fluids of the central nervous system, a substantial interference can result from the coexistence of uric acid (UA) and high concentrations of ascorbic acid because of their oxidation potentials on bare electrodes, which are close to that of DA, resulting in poor selectivity. Therefore, to obtain efficient and quick diagnostics, it is important to research and develop a highly selective and sensitive DA sensor.

Polyoxometalates (POMs), which are nanoscaled oxoclusters of transition metals that have intriguing structures and diverse properties, have been widely applied in several fields, including catalysis, medicine, magnetism, electrochromism, photochemistry, material science and nanotechnology [9–17]. Because of their multi-electron redox properties and high compositional stabilities, polyoxometalates are also used in electrochemical sensing; additionally, their physical properties can be fine tuned by varying the cationic constituents. In 2002, Kurth and coworkers used a polyoxometalate cluster, $[\text{Co}^{\text{II}}_4(\text{H}_2\text{O})_2\text{P}_4\text{W}_{30}\text{O}_{112}]^{16-}$ (Co-POM), to prepare pH-sensitive probes in self-assembled multilayers, creating a pathway to utilizing Co-POM as a molecular probe or to fabricate pH-sensitive microelectrodes [18]. In 2015, Xu and coworkers fabricated a nanocomposite film containing $\text{K}_6\text{P}_2\text{W}_{18}\text{O}_{62}$ (P_2W_{18}), carbon nanotubes (CNTs) and Au nanoparticles (Au NPs), which exhibited outstanding electrocatalytic capabilities for monitoring hydrogen peroxide as a modified electrode [19]. In 2018, a novel sandwich-type polyoxometalate (POM), which utilized $\text{Na}_{12}[\text{WCo}_3(\text{H}_2\text{O})_2(\text{CoW}_9\text{O}_{34})_2]$ and poly(vinyl imidazolium) cations $[\text{PVIM}^+]$ in combination with nitrogen-doped carbon nanotubes (NCNTs), was developed by the Mandal group for the highly selective and ultrasensitive detection of dopamine [20]. A polysaccharide biopolymer, chitosan (CHIT), poly- β -(1.4)-D-glucosamine, displayed an outstanding film-forming ability, high water permeability, good adhesion, and susceptibility to chemical modification due to the presence of reactive amino and hydroxyl functional groups. Additionally, chitosan possesses a primary amine at the C-2 position of the glucosamine residues and is soluble in aqueous acidic media at $\text{pH} < 6.5$. When chitosan is dissolved, it carries a positive charge on the $-\text{NH}_3^+$ groups, which enables it to adhere to negatively charged surfaces or adsorb negatively charged materials; thus, chitosan can be utilized as a cationic polyelectrolyte for the LbL assembly of films [21, 22]. Chitosan has been previously used in biosensors, materials science and food science [23, 24] due to its characteristics of excellent biodegradability, biocompatibility and nontoxicity [25–27].

In this paper, a composite film is reported that contains a Dawson-type polyoxometalate, $\alpha_2\text{-K}_7\text{P}_2\text{W}_{17}\text{VO}_{62}\cdot 18\text{H}_2\text{O}$, and chitosan; this film was prepared by a layer-by-layer (LbL) self-assembly method and employed as an electrochemical DA sensor. The as-prepared DA sensor demonstrates excellent amperometric sensing performance with a low detection limit, high sensitivity, wide linear range, and suitable response time as well as high stability for long-term application. In addition, this proposed DA sensor possesses the advantages of ease of fabrication and low cost. Scheme 1 illustrates the formation of the composite film.



Scheme 1. Scheme for the formation of the composite film $\{PEI/[P_2W_{17}V/CS]_n/P_2W_{17}V\}$.

2. EXPERIMENTAL DETAILS

2.1 Chemical

Poly(ethylenimine) (PEI MW 750,000) was acquired from Aldrich and used without further purification. The preparation of $\alpha_2\text{-K}_7\text{P}_2\text{W}_{17}\text{VO}_{62}\cdot 18\text{H}_2\text{O}$ ($P_2W_{17}V$) was performed based on the method reported in literature [28, 29] and identified by IR spectroscopy [30]. Additionally, without further treatment, chitosan (MW 100,000-300,000) was purchased from Aldrich with a deacetylation degree $\geq 95\%$. NaH_2PO_4 , Na_2HPO_4 , NaCl , acetic acid and H_2O_2 were purchased from Yongchang Chemical Company. Dopamine, uric acid, ascorbic acid and glucose were purchased from Aldrich. In all experiments, the water used was deionized and had a resistivity of $18\text{ M}\Omega$.

2.2 Instruments

All of the electrochemical experiments in this work were performed on a CHI760D Electrochemical Workstation (Shanghai Chenhua Instrument Corporation, China). Additionally, a traditional three-electrode system was used with Ag/AgCl as the reference electrode, twisted platinum wire as the counter, and a modified ITO electrode as the working electrode. With a U-3900 UV-Vis spectrophotometer from Hitachi (Japan), the UV-Vis absorption spectra were obtained on a quartz slide. Atomic force microscopy (AFM) images were taken by a AFM Dimension TM3100 manufactured by Digital Instruments (Santa Barbara, California, USA). XPS were collected on an ESCALAB-MKII spectrometer with $\text{Mg K}\alpha$ X-ray radiation as the X-ray source for excitation.

2.3 Preparation of the composite film

The preparation and characterization of the composite film $\{PEI/[P_2W_{17}V/CS]_n/P_2W_{17}V\}$ were performed on quartz slides, ITO-coated glass and silicon wafers. Based on the reported literature [31], the ITO-coated glass and quartz slides were wiped clean, while the silicon wafers were immersed in a

series of ultrasonically agitated solvents (acetone, ethanol, and H₂O) for 20 min to remove impurities. Then, the {PEI/[P₂W₁₇V/CS]_n/P₂W₁₇V} composite films were prepared as follows. To construct the precursor layer, a cleaned substrate was immersed in a solution of PEI (10 mM) followed by rinsing with deionized water and then drying under a nitrogen atmosphere. Then, the sample was alternately immersion for 30 min in a P₂W₁₇V (2 mM) solution and a CS (2 mg/ml) solution, and the precoated substrate was rinsed with deionized water following each immersion. This process was continued until reaching the desired number bilayers for {PEI/[P₂W₁₇V/CS]_n/P₂W₁₇V}.

3. RESULTS AND DISCUSSION

3.1 UV-Vis absorption spectra

The growth process of the {PEI/[P₂W₁₇V/CS]_n/P₂W₁₇V} composite film was monitored by UV-Vis spectroscopy. Figure 1(a) presents the UV-Vis absorption spectra of the {PEI/[P₂W₁₇V/CS]_n/P₂W₁₇V} (n = 1-6) composite film assembled on a quartz substrate (on both sides). All of the films have two characteristic absorption peaks in the UV region at 198 and 288 nm because of the oxygen-to-metal charge transfer (OMCT: O → W) in the P₂W₁₇V polyanions [32] and the absorption of chitosan [33]. Nevertheless, a slight shift in the band at 288 nm can be seen for the film compared with the P₂W₁₇V solution, as shown in Figure 1 (b). The electrostatic interaction between P₂W₁₇V and chitosan might result in the phenomenon. The inset of Figure 1 (a) plots the absorbance values at 198 and 288 nm with respect to the bilayer number, and the inset suggests that the growth in the deposition cycles is uniform and stable.

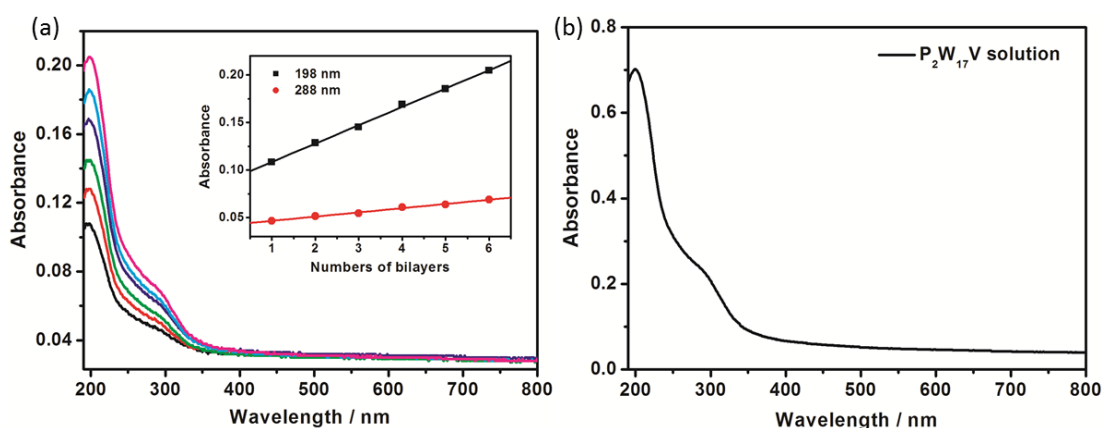


Figure 1. (a) UV-Vis absorption spectra of the {PEI/[P₂W₁₇V/CS]_n/P₂W₁₇V} composite film on a quartz substrate with n = 1-6; (b) UV-Vis absorption spectra of the P₂W₁₇V solution.

Based on the equation obtained from fitting the UV-Vis spectra, $\Gamma = (N_A A_\lambda) / 2n\epsilon_\lambda$, the surface coverage (Γ) of P₂W₁₇V can be obtained [34, 35], where N_A is Avogadro's constant, A_λ is the absorbance at a given wavelength, λ , ϵ_λ is the molar extinction coefficient (M⁻¹ cm⁻¹) and n is the

number of bilayers. In this paper, the surface coverage of the $\{\text{PEI}/[\text{P}_2\text{W}_{17}\text{V}/\text{CS}]_6/\text{P}_2\text{W}_{17}\text{V}\}$ film at 198 nm is $9.84 \times 10^{-11} \text{ mol cm}^{-2}$.

3.2 Structural and morphological characterization of the composite film

Detailed information on the surface morphology and the homogeneity of the composite film can be obtained by AFM, as presented in Figure 2. From the three-dimensional AFM image, the vertical grain structure on the surface of the composite can be obtained. The root-mean-square (rms) roughness of the composite film is 2.8 nm, which was calculated from the AFM image of a $1.0 \mu\text{m} \times 1.0 \mu\text{m}$ area.

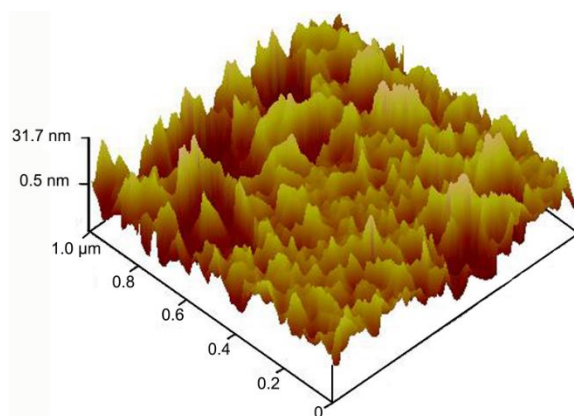


Figure 2. AFM image of the $\{\text{PEI}/[\text{P}_2\text{W}_{17}\text{V}/\text{CS}]_3/\text{P}_2\text{W}_{17}\text{V}\}$ composite film on a silicon wafer.

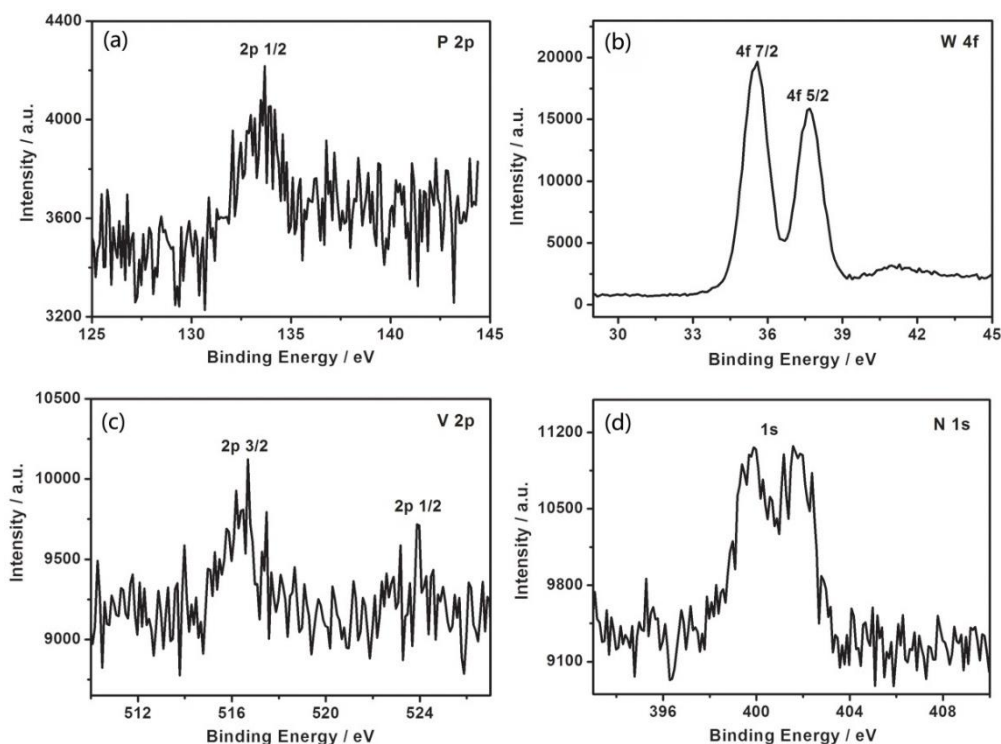


Figure 3. XPS spectra of the $\{\text{PEI}/[\text{P}_2\text{W}_{17}\text{V}/\text{CS}]_3/\text{P}_2\text{W}_{17}\text{V}\}$ composite film.

The composition of the LbL composite film was determined by X-ray photoelectron spectroscopy (XPS), as shown in Figure 3. Although the XPS measurements give only semiquantitative elemental compositions, peaks corresponding to P 2p (BE = 133.7 eV), W 4f_{7/2} (BE = 35.5 eV), W 4f_{5/2} (BE = 37.6 eV), V 2p_{3/2} (BE = 516.7 eV) and V 2p_{1/2} (BE = 523 eV) confirm the presence of P₂W₁₇V in the composite film. The splitting of the single N 1s peak at 399.9 and 401.7 eV reflects the oxidation states of the nitrogen atoms.

3.3 Electrochemical behavior of the composite film

The electrochemical behavior of the {PEI/[P₂W₁₇V/CS]₆/P₂W₁₇V} composite film was studied by cyclic voltammetry in 0.05 M PBS (pH = 7.0). The CV curves of the composite film at different scan rates in the potential range of -1.0 to 0.8 V are shown in Figure 4. The {PEI/[P₂W₁₇V/CS]₆/P₂W₁₇V} composite film presents three pairs of strong redox peaks with mean peak potentials, E_{1/2}, of -0.5155, -0.7517 and -0.9495 V, and two pairs of very weak redox peaks with mean peak potentials, E_{1/2}, of 0.4908 and -0.3985 V. Pair I represents a one-electron redox peak, which is attributed to the vanadium center (V^V → V^{IV}) [34, 35], as shown in the upper inset, and the two one-electron redox peaks of the tungsten center (W^{VI} → W^V) are labelled as pairs II and III [36]. The CV curves of the composite film prove that the electrochemical properties of P₂W₁₇V are totally preserved in the composite film. As the scan rate increases (from 100 to 450 mV s⁻¹), a reversible but nonideal redox process can be observed, for which the anodic peak potentials shift to positive values and the cathodic peak potentials shift to negative values. Taking peak IV as an example, the linear relationship between the scan rate and the square root of the peak current was analyzed. For the scan rate and the square root of the peak current, linear regression equations could be obtained as follows: I_{a1} (mA) = 15.47228 (mV s⁻¹)^{1/2} - 97.4693, $R_{a1}^2 = 0.9966$ for the anodic peak, and I_{c1} (mA) = -19.17281 (mV s⁻¹)^{1/2} + 60.14017, $R_{c1}^2 = 0.9936$ for the cathodic peak. For the peak current and scan rate, the linear regression equations could be calculated as follows: I_{a2} (mA) = 0.49061 (mV s⁻¹) + 17.9591, $R_{a2}^2 = 0.9967$ for the anodic peak, and I_{c2} (mA) = -0.60892 (mV s⁻¹) - 62.62817, $R_{c2}^2 = 0.9968$ for the cathodic peak. The R_{a2}^2 and R_{c2}^2 values are closer to 1 than those of R_{a1}^2 and R_{c1}^2 , which indicates that the electrochemical redox of the composite film is a surface-confined electrochemical process. The relationship between the scan rate and the current is shown in the lower inset of Figure 4.

The surface coverage (Γ) of P₂W₁₇V can be calculated based on the following equation: $\Gamma = 4i_pRT/n^2F^2vA$, where i_p is the peak current (A), R is the molar gas constant, T is the thermodynamic temperature, n is the number of electrons transferred per electroactive species, F is the Faraday constant, v is the scan rate (V s⁻¹), and A is the geometric area of the working electrode (cm²). The surface coverage of P₂W₁₇V per layer is calculated to be 7.94×10^{-11} mol cm⁻² for the {PEI/[P₂W₁₇V/CS]₆/P₂W₁₇V} composite film based on analyzed cyclic voltammograms measured at a scan rate of 100 mV s⁻¹. This result is in agreement with the surface coverage of 9.84×10^{-11} mol cm⁻² measured by UV-Vis spectroscopy.

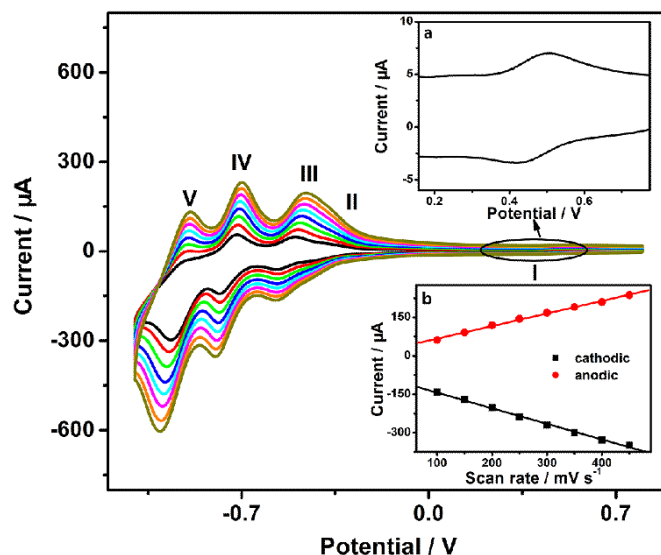


Figure 4. CV curves of the {PEI/[P₂W₁₇V/CS]₆/P₂W₁₇V} composite film at different scan rates (100, 150, 200, 250, 300, 400 and 450 mV s⁻¹). Inset a: enlargement of the elliptic region. Inset b: the relationship between scan rate and current. Reference electrode: Ag/AgCl.

The interfacial properties of the composite film were studied using electrochemical impedance spectroscopy (EIS). The complex impedance consists of two parts, the real (Z_{re}) component and the imaginary (Z_{im}) component. At the composite film interface, the diameter of the semicircle in EIS is equivalent to the electron transfer resistance (R_{et}), by which the electron transfer kinetics of the redox can be controlled [37]. The typical results of the impedance behaviors of the {PEI/[P₂W₁₇V/CS]_n/P₂W₁₇V} ($n = 2, 4, 6$ and 8) composite film are shown in Figure 5. Two semicircles exist for each film. At high frequencies, small semicircles are observed, followed by second larger capacitive loops at lower frequencies. The presence of the film covering the surface of the electrode leads to the formation of small semicircles, and the electron transfer resistance and double-layer capacitance of the electrode can account for the development of the second larger semicircles. In addition, as the bilayer number of the composite film increases from 2 to 8, the diameter of the semicircular regions decreases gradually, which proves that augmenting the surface coverage of the P₂W₁₇V polyanions can improve the electron transfer capability of the composite film.

For impedance spectroscopy, the electrode system can be simplified as an equivalent circuit fit to the obtained impedance data of the {PEI/[P₂W₁₇V/CS]₆/P₂W₁₇V} composite film, as shown in the inset of Figure 5. In this simple equivalent circuit, both the relationship between the resistance to charge transfer (R_1) and the constant phase element (CPE1) and that of the capacitance of the surface layer (CPE2) and the film resistance (R_2) are in parallel. This parallel relationship of R_1 and CPE1 as well as that of R_2 and CPE2 results in a semicircle in the complex plane of the plot of Z_{im} versus Z_{re} . On the basis of the impedance spectrum, R_1 and CPE1 were 4556 Ω and 3.7598×10^{-4} F, respectively. At the interface of the {PEI/[P₂W₁₇V/CS]₆/P₂W₁₇V} composite film, the electric charge-transmission speed constant (k) of W⁵⁺/W⁶⁺ can be calculated by the following equation [38, 39]:

$$k = \frac{RT}{R_1 C_n^2 F^2 A}$$

where the resistance to charge transfer is represented by R_1 , the number of electrons transferred per electroactive species is represented by n , the constant phase element (CPE1) is represented by C , the geometric area of the electrode is represented by A , and all other terms have their usual meaning.

Based on this equation, the electric charge-transmission speed constant (k) of the $\{\text{PEI}/[\text{P}_2\text{W}_{17}\text{V}/\text{CS}]_6/\text{P}_2\text{W}_{17}\text{V}\}$ composite film was calculated to be $1.94 \times 10^{-5} \text{ cm s}^{-1}$.

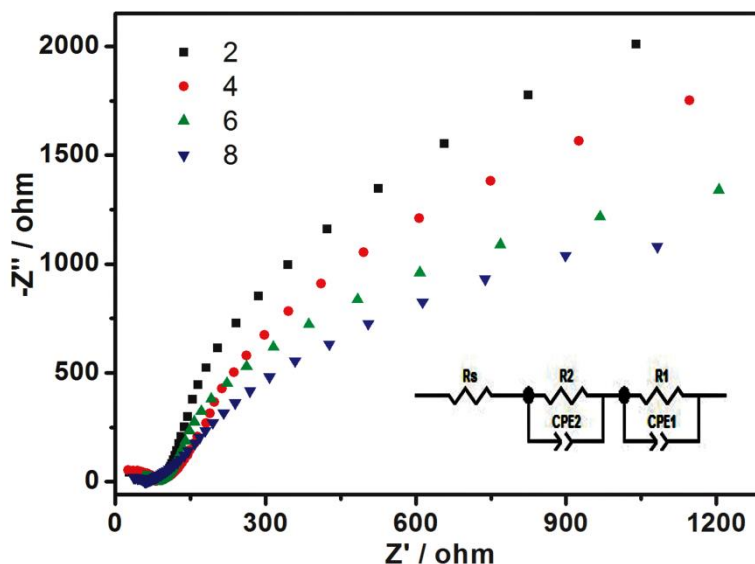


Figure 5. The EIS of the $\{\text{PEI}/[\text{P}_2\text{W}_{17}\text{V}/\text{CS}]_n/\text{P}_2\text{W}_{17}\text{V}\}$ composite films with $n = 2, 4, 6$ and 8 in $0.05 \text{ M PBS (pH = 7.0)}$. Inset: the equivalent circuit.

3.4 Electrocatalytic activity of the composite film

The catalytic efficiency can be impacted by the bilayer number of the composite film. A sequence of parallel electrocatalytic experiments of $\{\text{PEI}/[\text{P}_2\text{W}_{17}\text{V}/\text{CS}]_n/\text{P}_2\text{W}_{17}\text{V}\}$ composite films with different bilayer numbers ($n = 4, 6, 8, 10$ and 12) towards the oxidation of DA were performed. The CV voltammograms of the $\{\text{PEI}/[\text{P}_2\text{W}_{17}\text{V}/\text{CS}]_6/\text{P}_2\text{W}_{17}\text{V}\}$ composite films in $0.05 \text{ M PBS (pH = 7.0)}$ with varying concentrations of DA are shown in Figure 6. Upon the addition of DA, strong catalytic peaks appear at 0.57 V , which indicate that the composite films can electrocatalyze the oxidation of DA. The inset of Figure 6 shows that the catalytic current increases with increasing concentrations of DA, which suggests that this composite can be developed for potential applications in the detection of DA.

The catalytic efficiency can be calculated according to the following formula [40]: $\text{CAT} = 100\% \times [I_p(\text{POM, DA}) - I_p(\text{POM})] / I_p(\text{POM})$, where $I_p(\text{POM, DA})$ is the peak current of the POM in the presence of DA, and $I_p(\text{POM})$ is the peak current without the presence of DA. When the DA concentration is 0.05 mM , the electrocatalytic efficiencies of the $\{\text{PEI}/[\text{P}_2\text{W}_{17}\text{V}/\text{CS}]_n/\text{P}_2\text{W}_{17}\text{V}\}$ composite films with $n = 4, 6, 8, 10$ and 12 are 192.61% , 532.48% , 316.63% , 385.64% and 277.37% , respectively (the CVs of the $\{\text{PEI}/[\text{P}_2\text{W}_{17}\text{V}/\text{CS}]_n/\text{P}_2\text{W}_{17}\text{V}\}$ ($n=2, 4, 8, 10$ and 12) composite films in $0.05 \text{ M PBS (pH = 7.0)}$ containing DA at various concentrations are not given here. The results above

indicate that the composite film with a 6-bilayer structure has the highest catalytic efficiency of the studied films. Hence, in the follow experiments, a 6-bilayer composite film was selected as the working electrode to guarantee a high catalytic efficiency for the as-prepared sensor.

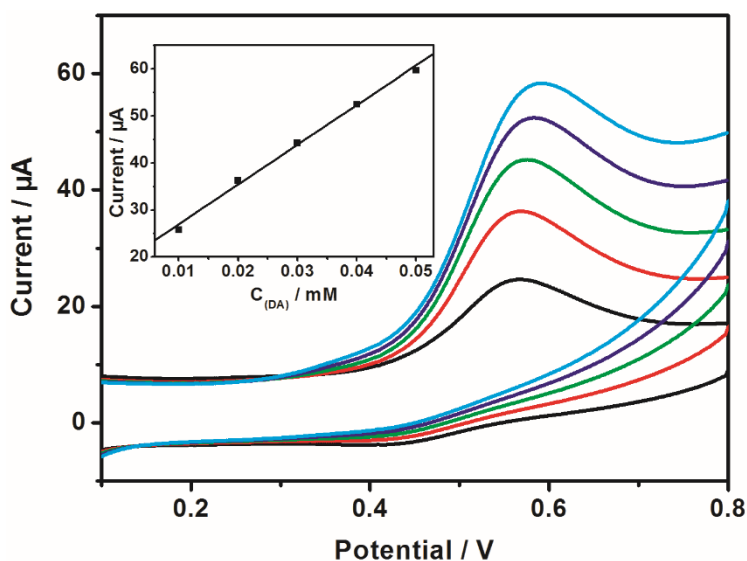
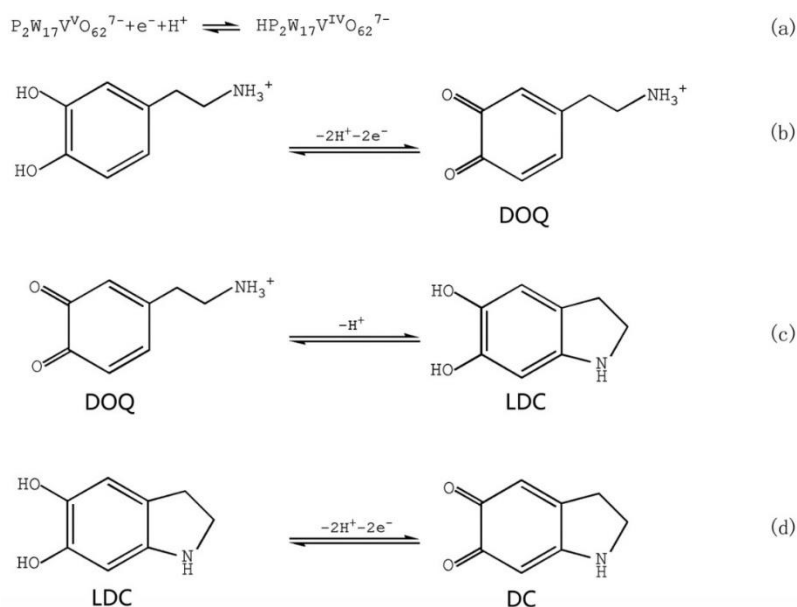


Figure 6. The CV voltammograms of the {PEI/[P₂W₁₇V/CS]₆/P₂W₁₇V} composite film in 0.05 M PBS (pH = 7.0) containing various concentrations of DA. The inset shows the relationship between the catalytic current and the concentration of DA.

The mechanism for the electrochemical redox of DA by a {PEI/[P₂W₁₇V/CS]₆/P₂W₁₇V} composite film can be expressed as the equations that follow in Scheme 2[41–44]:



Scheme 2. The mechanism for the electrochemical redox of DA by a {PEI/[P₂W₁₇V/CS]₆/P₂W₁₇V} composite film.

According to the above mechanism, DA is transformed into dopamine ortho-quinone (DOQ) through a two-proton and two-electron process (b-in Scheme 2). The polyoxometalate serves as a

proton and electron reservoir (a-in Scheme 2) to mediate this process. The amine group of the produced DOQ exists in its unprotonated state under weakly acidic or neutral conditions, and undergoes a cyclization process to produce leucodopaminechrome (LDC) (c-in Scheme 2). Afterwards, at less-positive potentials, LDC is oxidized in a similar two-electron and two-proton process to produce dopaminechrome (DC) (d-in Scheme 2). In the composite film, due to the presence of the $P_2W_{17}V$ anions, the kinetics of the electrochemical oxidation are enhanced, and a faster electron transfer rate is obtained.

3.5 Analytical evaluation of the DA sensor

3.5.1 Amperometric detection of DA

Amperometry was used to examine the sensing characteristics of a $P_2W_{17}V/CS$ film deposited on an ITO electrode for the determination of dopamine. As shown in Figure 7 (a), at an applied potential of 0.57 V, a current response was generated by adding 3.04×10^{-4} M DA to a stirring solution of 0.05 M PBS (pH = 7.0), and the insets in Figure 7a show the enlargements of both the one-step addition of DA and the current-time curve between 1 and 250 s. Once DA had been added, a rapid current response occurred, and the current signal reached the steady-state current within 2.2 s. A well-defined and stable amperometric response, taken at 50 s intervals, was obtained through 2100 s. As shown in Figure 7 (b), the catalytic current increases linearly with increasing concentrations of DA, and the linear detection range is from 1.25×10^{-8} to 3.04×10^{-4} M. The linear regression equation for the catalytic current versus concentration of DA is I_{DA} (mA) = $0.22947 \times C_{DA}$ (mM) - 0.63422, with a correlation coefficient of 0.998. The sensitivity of the composite film was determined to be $0.23 \mu A \mu M^{-1}$ for the detection of DA, and the detection limit was estimated to be $0.18 \mu M$. The sensory characteristics of the composite film were compared with several previously reported DA sensors, and the comparison results are summarized in Table 1.

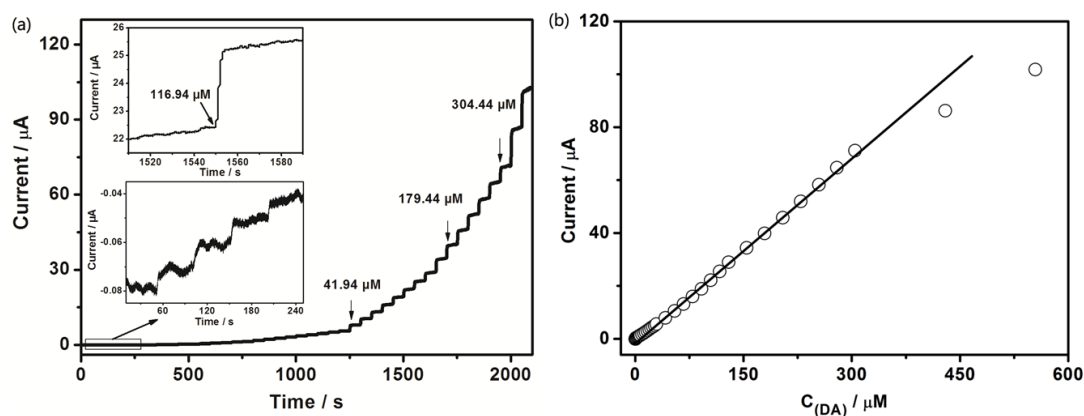


Figure 7. (a) Typical current-time curve of a $\{PEI/[P_2W_{17}V/CS]_6/P_2W_{17}V\}$ -modified electrode upon successive additions of DA at an applied potential of 0.57 V vs. Ag/AgCl in 0.05 M PBS (pH = 7.0) and (b) calibration plot of the steady-state currents obtained for the $\{PEI/[P_2W_{17}V/CS]_6/P_2W_{17}V\}$ composite film versus the concentrations of DA.

Table 1. Comparative characteristics of the as-prepared sensor and previously reported sensors for the determination of dopamine.

Electrode	Limit of detection (μM)	Linear range (M)	Potential (V)	Reference
Au/Gr-AuAg	0.205	$3.0 \times 10^{-7} - 3.0 \times 10^{-4}$	0.24	[41]
Au/Gr-Au	30.3	$10^{-5} - 10^{-4}$	0.24	[41]
LDH/CoPcTs	0.32	$2.0 \times 10^{-5} - 1.4 \times 10^{-4}$	0.64	[37]
Capillary-to-electrode	0.45	$5.0 \times 10^{-7} - 5.0 \times 10^{-4}$	0.9	[45]
PEDOT-modified electrode	0.1	$2.0 \times 10^{-7} - 3.0 \times 10^{-4}$	0.15	[46]
t-GN-Au/GCE ^a	0.057	$0.8 \times 10^{-6} - 2.0 \times 10^{-3}$	0.4	[47]
PMO ₉ V ₃ -Pt-modified electrode	0.13	$4.2 \times 10^{-7} - 1.3 \times 10^{-3}$	0.8	[48]
[PMO ₁₁ V/PEI/CoPcTs] ₄ /ITO ^b	0.013	$8.3 \times 10^{-8} - 5.0 \times 10^{-4}$	0.9	[49]
[P ₂ W ₁₇ V/CS] ₆ /ITO ^b	0.18	$1.25 \times 10^{-8} - 3.04 \times 10^{-4}$	0.57	This work

^a Glass carbon electrode^b Indium Tin Oxide

3.5.2 Selectivity and sensitivity

The electric potential determines the selectivity of an electrochemical sensor. Therefore, the current responses of four interference species (AA, UA, glucose and H₂O₂) along with DA were tested for the {PEI/[P₂W₁₇V/CS]₆/P₂W₁₇V} composite film at different applied potentials. From Figure 8, it can be seen that the catalytic current of DA oxidation increases with a positive shift of the applied potential, showing that not only the selectivity but also the sensitivity of the sensor is effected by the applied potential. The more positive the applied potential is, the higher the sensitivity of sensor. On the other hand, at a positive potential of +0.57 V, 3.36% and 9.72% of the anodic current response of 2.5 μM solutions of UA and AA were detected relative to a 2.5 μM solution of DA. Almost no current response was detected at these applied potentials for glucose and H₂O₂, and the as-prepared sensor showed good selectivity and sensitivity. A low potential, +0.57 V (vs. Ag/AgCl), was chosen as the optimized applied potential for the detection of DA in the following experiments.

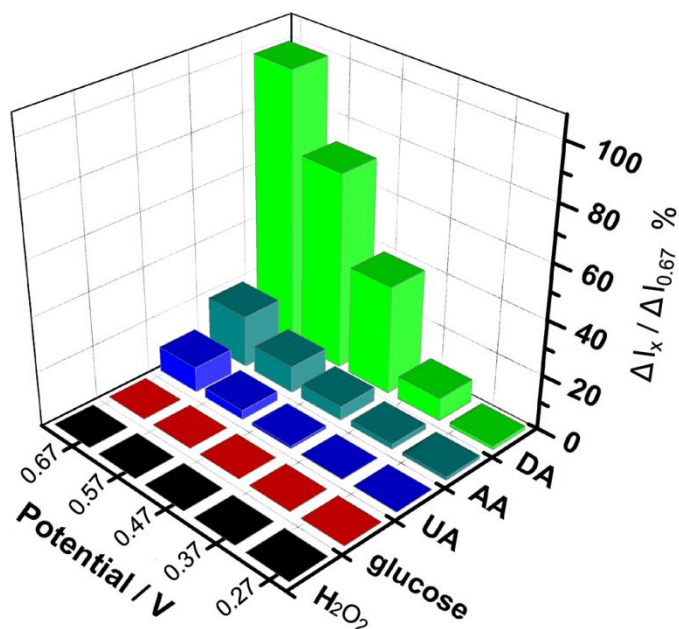


Figure 8. The selectivity profile of the composite film obtained using 2.5 μM solutions of DA, AA, UA, glucose and H_2O_2 at different applied potentials: 0.27, 0.37, 0.47, 0.57 and 0.67 V in 0.05 M PBS (pH = 7.0).

3.5.3 Stability and reproducibility properties of the composite film

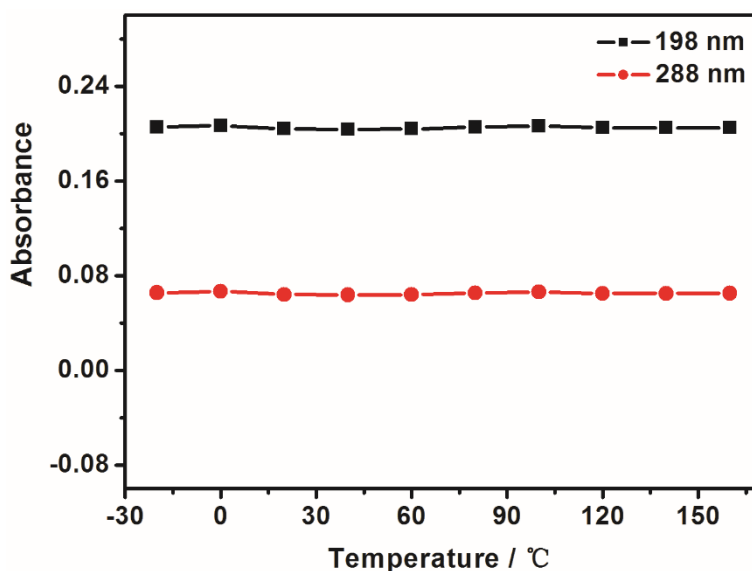


Figure 9. The absorbance of the $\{\text{PEI}/[\text{P}_2\text{W}_{17}\text{V}/\text{CS}]_6/\text{P}_2\text{W}_{17}\text{V}\}$ composite film at 198 nm and 288 nm at various temperatures.

To examine the thermal stability of the composite film, UV-Vis spectra were recorded after heating (or cooling) under various temperatures. The results suggest that the composite film has excellent thermal stability, even after heating to 160 °C (see Figure 9). In addition, the stability of the $\{\text{PEI}/[\text{P}_2\text{W}_{17}\text{V}/\text{CS}]_6/\text{P}_2\text{W}_{17}\text{V}\}$ composite film was determined by cyclic voltammetry, which was

sampled over 100 cycles, and very little loss in the response current signal was observed, as shown in Figure 10. The film-to-film reproducibility was tested in 0.05 M PBS with 10 μM DA utilizing various composite films fabricated under the same conditions. The excellent reproducibility can be verified by the small relative standard deviation of 3.6%.

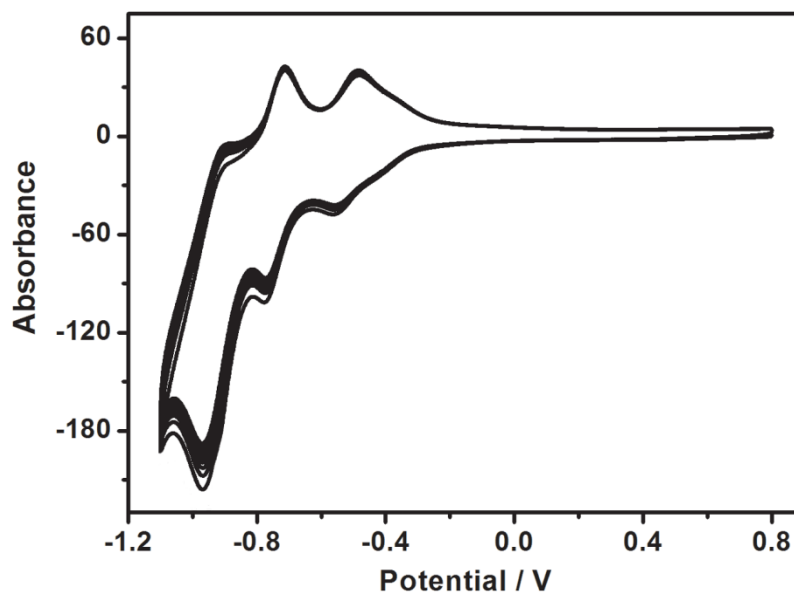


Figure 10. Cyclic voltammograms of the $\{\text{PEI}/[\text{P}_2\text{W}_{17}\text{V}/\text{CS}]_6/\text{P}_2\text{W}_{17}\text{V}\}$ composite film over 100 cycles in a 0.05 M PBS solution (pH = 7.0). Scan rate: 100 mV s^{-1} .

3.6 Determination of DA in a real sample

Using the standard addition method, we selected human serum samples as the biological samples to be analyzed. All samples were diluted with 0.05 M PBS (pH 7.0). The recoveries of the spiked samples ranged from 96.00-102.07%, as shown in Table 2. Thus, in real samples, the proposed method may provide a feasible tool for the determination of DA.

Table 2 Results of the recovery tests obtained for the determination of DA in a real sample.

Sample	$C_{\text{DA}}/(\mu\text{M})$ (added)	$C_{\text{DA}}/(\mu\text{M})$ (found)	Recovery (%)
1	5.0	4.80	96.00
2	10.0	9.96	99.60
3	15.0	15.31	102.07
4	20.0	20.27	101.35
5	25.0	24.64	98.60

4. CONCLUSIONS

In summary, a novel sensing composite film for the detection of DA in aqueous solutions, which was based on the two functional components of $\text{P}_2\text{W}_{17}\text{V}$ and CS, was successfully prepared

according to a LbL strategy. The composite film with 6 bilayers had the highest catalytic efficiency. The as-prepared films are noble metal free, low cost, and easy to prepare compared with many other composites used for electroanalysis. With its excellent selective, sensitive, stable and fast amperometric response, the composite film can be considered an appropriate material for the detection of DA. Under the experimental conditions, the concentration range for linear detection is 1.25×10^{-8} M to 3.04×10^{-4} M, the detection limit is 0.18 μ M (S/N = 3), and the response time is 2.2 s. The results indicate that composite films containing the Dawson-type polyoxometalate $P_2W_{17}V$ represent promising materials for future applications in amperometric sensors. This composite film system, {PEI/[$P_2W_{17}V$ /CS] $_6$ / $P_2W_{17}V$ }, can be employed as a unique device for the detection of DA.

ACKNOWLEDGMENTS

This work was financially supported by the NSF of China (21701037), youth scholar backbone supporting plan project for general universities of Heilongjiang Province (1254G020) and Postdoctoral Science Foundation, China (2017M611380).

References

1. R. Wightman, C. Amatorh, R. Engstrom, P. Hale, E. Kristensen, W. Kubr and L. May, *Neuroscience*, 25 (1998) 513-523.
2. N. Li, Y. Lu, S. Li, Q. Zhang, J. Wu, J. Jiang, G.L. Liu and Q. Liu, *Biosens. Bioelectron.*, 93 (2017) 241-249.
3. S. Mahshid, C.C. Li, S.S. Mahshid, M. Askari, A. Dolati, L.X. Yang, S.L. Luo and Q.Y. Cai, *Analyst*, 136 (2011) 2322-2329.
4. P.S. Rao, N. Rujikarn, J.M. Lubner and D.H. Tyras, *Chromatographia*, 28 (1989) 307-310.
5. M.A. Fotopoulou and P.C. Ioannou, *Anal. Chim. Acta*, 462 (2002) 179-185.
6. R.M. Cheng, C.C. Ge, L. Qi, Z.Y. Zhang, J.L. Ma, H.Y. Huang, T.H. Pan, Q.B. Dai and L.M. Dai, *J. Phys. Chem. C*, 122 (2018) 13314-13321.
7. S.T. Barlow, M. Louie, R. Hao, P.A. Defnet and B. Zhang, *Anal. Chem.*, 90 (2018) 10049-10055.
8. Z.W. Jiang, P.F. Gao, L. Yang, C.Z. Huang and Y.F. Li, *Anal. Chem.*, 87 (2015) 12177-12182.
9. W.L. Sun, B.W. An, B. Qi, T. Liu, M. Jin and C.Y. Duan, *ACS Appl. Mater. Interfaces*, 10 (2018) 13462-13469.
10. V. Singh, S.D. Adhikary, A. Tiwari, D. Mandal and T.C. Nagaiah, *Chem. Mater.*, 29 (2017) 4253-4264.
11. M.A.R. Anjum and J.S. Lee, *ACS Catal.*, 7 (2017) 3030-3038.
12. R.J. Liu, G.J. Zhang, H.B. Cao, S.J. Zhang, Y.B. Xie, A. Haider, U. Kortz, B.H. Chen, N.S. Dalal, Y.S. Zhao, L.J. Zhi, C.X. Wu, L.K. Yan, Z.M. Su and B. Keita, *Energy Environ. Sci.*, 9 (2016) 1012-1023.
13. C.T. Buru, P. Li, B.L. Mehdi, A. Dohnalkova, A.E. Platero-Prats, N.D. Browning, K.W. Chapman, J.T. Hupp and O.K. Farha, *Chem. Mater.*, 29 (2017) 5174-5181.
14. D.Y. Du, J.S. Qin, S.L. Li, Z.M. Su and Y.Q. Lan, *Chem. Soc. Rev.*, 43 (2014) 4615-4632.
15. S.B. Li, L. Zhang, Y.Q. Lan, K.P. O'Halloran, H.Y. Ma and H.J. Pang, *Chem. Commun.*, 54 (2018) 1964-1967.
16. C. Chen, B.X. Li, L.J. Zhou, Z.F. Xia, N.J. Feng, J. Ding, L. Wang, H. Wan and G.F. Guan, *ACS Appl. Mater. Interfaces*, 9 (2017) 23060-23071.
17. H.P. Ma, B.L. Liu, B. Li, L.M. Zhang, Y.G. Li, H.Q. Tan, H.Y. Zang and G.S. Zhu, *J. Am. Chem. Soc.*, 138 (2016) 5897-5903.
18. S.Q. Liu, D.G. Kurth and D. Volkmer, *Chem. Comm.*, (2002) 976-977.
19. S.Y. Guo, L. Xu, B.B. Xu, Z.X. Sun and L.H. Wang, *Analyst*, 140 (2015) 820-826.

20. N. Thakur, S.D. Adhikary, M. Kumar, D. Mehta, A.K. Padhan, D. Mandal and T.C. Nagaiah, *ACS Omega*, 3 (2018) 2966-2973.
21. B. Krajewska, *Enzyme Microb. Technol.*, 35 (2004) 126-139.
22. D.W. Fan and J.C. Hao, *J. Phys. Chem. B*, 113 (2009) 7513-7516.
23. P. Sahariah and M. Másson, *Biomacromolecules*, 18 (2017) 3846-3868.
24. H.V. Duong, T.T. L. Chau, N.T.T. Dang, F. Vanterpool, M. Salmerón-Sánchez, E. Lizundia, H.T. Tran, L.V. Nguyen and T.D. Nguyen, *ACS Omega*, 3 (2018) 86-95.
25. P. Sahariah, M. Másson and R.L. Meyer, *Biomacromolecules*, 19 (2018) 3649-3658.
26. H.X. Wang, J. Qian and F.Y. Ding, *J. Agric. Food Chem.*, 66 (2018) 395-413.
27. H.Q. Le, Y. Sekiguchi, D. Ardiyanta and Y. Shimoyama, *ACS Omega*, 3 (2018) 14103-14110.
28. M. Abbessi, R. Contant, R. Thouvenot and G. Hervé, *Inorg. Chem.*, 30 (1991) 1695-1702.
29. B. Keita, E. Abdeljalil, L. Nadjo, B. Avisse, R. Contant, J. Canny and M. Richet, *Electrochem. Commun.*, 2 (2000) 145-149.
30. S.P. Harmalker, M.A. Leparulo and M.T. Pope, *J. Am. Chem. Soc.*, 105 (1983) 4286-4292.
31. L. Kang, H.Y. Ma, Y. Yu, H.J. Pang, Y.B. Song and D. Zhang, *Sens. Actuators, B*, 177 (2013) 270-278.
32. D. Zhang, Y.Y. Chen, H.J. Pang, Y. Yan and H.Y. Ma, *Electrochimica Acta*, 105 (2013) 560-568.
33. Y.H. Wang, C.X. Guo, Y.W. Chen, C.W. Hu and W.H. Yu, *J. Colloid Interface Sci.*, 264 (2003) 176-183.
34. B. Keita, I.M. Mbomekalle, L. Nadjo, P. Oliveira, A. Ranjbari, R. Contant and C.R. Chime., *J. Cluster Sci.*, 8 (2005) 1057-1066.
35. P. Wang, X.P. Wang, L.H. Bi and G.Y. Zhu, *J. Electroanal. Chem.*, 495 (2000) 51-56.
36. B. Keita, F. Girard, L. Nadjo, R. Contant, J. Canny and M. Richet, *J. Electroanal. Chem.*, 478 (1999) 79-82.
37. J.B. Han, X.Y. Xu, X.Y. Rao, M. Wei, D.G. Evans and X. Duan, *J. Mater. Chem.*, 21 (2011) 2126-2130.
38. E. Sabatani and I. Rubinstein, *J. Phys. Chem.*, 91 (1987) 6663-6669.
39. L. Chen, L. Tian, L. Liu, X.F. Tian, W.B. Song, H.D. Xu and X.H. Wang, *Sens. Actuators, B.*, 110 (2005) 271-278.
40. A.M. Khenkin, L. Weiner, Y. Wang and R. Neumann, *J. Am. Chem. Soc.*, 123 (2001) 8531-8542.
41. S. Pruneanu, A.R. Biris, F. Pogacean, C. Socaci, M. Coros, M.C. Rosu, F. Watanade and A.S. Biris, *Electrochim. Acta*, 154 (2015) 197-204.
42. X.F. Gu, G.M. Jiang, G.Q. Jiang, T.T. Chen, W.Y. Zhan and X. Li, *Talanta*, 137 (2015) 189-196.
43. H.M. Cheng, H. Qiu, Z.W. Zhu, M.X. Li and Z.J. Shi, *Electrochim. Acta*, 63 (2012) 83-88.
44. M. Sadakane and E. Steckhan, *Chem. Rev.*, 98 (1998) 219-237.
45. C.W. Cheng, K.L. Lee, S.S. Chang, D.C. Chen, C.M. Yu and C. Chen, *Anal. Chem.*, 74 (2002) 3906-3910.
46. F.S. Belaidi, A. Civelas, V. Castagnola, A. Tsopela, L. Mazonq, P. Gros, J. Launay and P. Temple-Boyer, *Sens. Actuators, B.*, 214 (2015) 1-9.
47. C. Li, J. Zhao, X. Yan, Y. Gu, W. Liu, L. Tang, B. Zheng, Y. Li, R. Chen and Z. Zhang, *Analyst*, 140 (2015) 1913-1920.
48. S. Li, H.Y. Ma, K.P. O' Halloran, H.J. Pang and H.R. Ji, *Electrochim. Acta*, 108 (2013) 717-726.
49. W. Zhu, W.J. Zhang, S. Li, H.Y. Ma, W. Chen and H.J. Pang, *Sens. Actuators, B.*, 181 (2013) 773-781.